

CASE STUDIES OF ENGINEERING AND ENVIRONMENTAL APPLICATIONS OF INDUCED POLARIZATION IMAGING

Lee Slater*, Andrew Binley[^] and Andreas Kemna[†]

* Department of Geosciences, University of Missouri - Kansas City,
5100 Rockhill Road, Kansas City, Missouri 64110

[^] Department of Environmental Science, Lancaster University, Lancaster, LA1 4YQ, England

[†] Institute of Chemistry and Dynamics of the Geosphere, Research Center Juelich,
D-52425 Juelich, Germany; *formerly*: DMT, GeoTec Division, Am Technologiepark 1,
D-45307 Essen, Germany

ABSTRACT

Induced polarization (IP) imaging is a relatively new geophysical method in engineering studies. We document three test studies conducted to evaluate the potential of the method when structural properties of the subsurface are required, such as in highway design and bridge construction. Our studies illustrate the application of IP for resolving lithology, as well as hydraulic conductivity and hydrocarbon contamination. Fundamentally, the IP response depends on microgeometry and mineralogy, as well as fluid chemistry and saturation. We show that IP imaging is a promising tool for mapping lithological contrasts in unconsolidated sediments. However, the range of IP response observed in these sediments complicates lithological interpretation. At one site, high polarization correlates with clayey sediments identified from gamma logging. Here, these clays are considered disseminated throughout sand/silt/gravel units. At a second site, the sequence of Quaternary sediments is more complex. Difficulties in lithological interpretation arise as no simple relation between clay content and polarization is evident. Our work identifies the need for further laboratory investigations to better understand the effects of microgeometry and mineralogy on polarization. Other laboratory studies have identified the possibility of predicting hydraulic permeability and hydrocarbon content from IP measurements. In a third study, we describe the results of IP imaging at a hydrocarbon-contaminated site. The hydrocarbon location is evident from the IP image. At this site, we also attempt to predict hydraulic permeability variability from the IP data. The resulting permeability image correlates well with known lithological variability at the site. However, further laboratory work is needed to improve models relating hydrocarbon contamination and hydraulic permeability to electrical parameters. Given recent advances in data acquisition systems and imaging algorithms, we anticipate an increase in engineering-related applications of the IP method.

1. INTRODUCTION

The Induced Polarization (IP) method is an exploration tool that, until recently, has primarily been used for mineral exploration. However, environmental and engineering applications of the IP method have emerged from laboratory studies of measurable IP effects associated with non-metallic minerals (Olhoeft, 1985; Vanhala and Soininen, 1995; Börner et al., 1996). It is now known that the interface between a non-metallic mineral and a saturating fluid polarizes as a result of redistribution of ions along the interface following application of an electric current. Upon current termination, ions relax to the equilibrium condition, the resulting residual current flow being the source of the subsurface IP response. The magnitude of this polarization is a function of numerous factors, and further research is required to adequately model this diffusion-controlled relaxation. Previous work shows that the IP magnitude is closely related to microgeometrical properties, particularly the surface area available for polarization (Börner and Schön, 1991) and the surface charge density. Vanhala (1997) showed that for unconsolidated sediments ranging from gravel to fine silt, the IP effect is closely related to modal grain size, with IP increasing as grain size decreases. However, mineralogy, fluid chemistry and saturation also influence this polarization and complicate interpretation (Klein and Sill, 1982; Vinegar and Waxman, 1984; Vanhala et al., 1992). A strong IP effect is observed in sediments containing

clays disseminated on the surface of larger grains. Hence, shaly sand/silt and shaly sandstone typically display large IP effects (Klein and Sill, 1982; Sturrock et al., 1998). In contrast, compacted clays are usually associated with low IP effects, as ohmic conduction dominates current flow. Small but measurable IP effects are associated with clean sand and gravel (Vanhala, 1997).

Potential engineering and environmental applications of IP are numerous. Given the strong dependence of IP on microgeometry and mineralogy, it should be possible to use IP as a tool for lithological discrimination. The method could hence assist subsurface characterization in advance of emplacement of a large engineering structure, such as a bridge. Recognizing the importance of surface area on fluid flow, workers have also investigated the possibility of using IP to estimate the hydraulic permeability of sandstone and unconsolidated sediments. Furthermore, it is known that the presence of organic contaminants can modify the impedance of the fluid-grain interface through clay polymerization (Olhoeft, 1985; Vanhala, 1997). A promising environmental application of the IP method is hence the detection of organic contaminants, notoriously difficult targets for detection using other geophysical methods.

Recent advances in IP instrumentation and modeling algorithms, combined with a better understanding of the physical significance of the IP response, encourages field-scale engineering applications of the method. Within the last 10 years, a 'revolution' in the application of the resistivity method occurred with development of multi-electrode, automated data acquisition systems and 2D (recently 3D) inversion algorithms for resistivity image reconstruction. Engineering and environmental applications of the resistivity method escalated as a result of these technological advances, which facilitate visualization of the subsurface resistivity distribution. In recent years, this technology has been extended to 'upgrade' the IP method. Instrumentation and software now exist, making it possible to obtain 2D or 3D images of the polarizability of the subsurface.

In this paper, we document three studies conducted to evaluate IP imaging as a tool in engineering and environmental investigations. These studies address the key identified potential near-surface applications of the IP method, namely lithological characterization, hydraulic conductivity estimation and hydrocarbon detection. We emphasize the role of IP in lithologic studies, as this is fundamental to bridge design and highway construction. We illustrate the method as applied from a conventional surface array of electrodes and as applied using electrodes placed in boreholes. Between borehole measurements much improve image resolution, particularly at depth. Although our studies illustrate the potential value of the method, image reconstruction software capable of handling borehole electrodes is not yet commercially available.

We find that, with careful interpretation, IP imaging can improve our understanding of the engineering properties of the subsurface relative to resistivity imaging alone. However, our studies also indicate that further laboratory data are needed to better understand the effects of microgeometry, mineralogy, fluid chemistry and saturation on the IP response. Field-scale imaging of the distribution of hydraulic conductivity or hydrocarbons appears a promising application of the method.

2. INVESTIGATION OF LITHOLOGY USING SURFACE IP IMAGING

Background

Much of Denmark is covered with a blanket of fluvial and glacial unconsolidated sediments, which exhibit heterogeneity over a range of scales. Lithological mapping using pulled-array DC-resistivity and electromagnetic methods has met with considerable success (Christensen and Sorensen, 1998; Poulsen and Christensen, 1999). However, resolution of clayey sediments from clean sand and gravel has been complicated by the strong dependence of earth resistivity on fluid chemistry and saturation, in addition to lithology.

A field test was conducted to determine the value of IP in resolving lithological variability in such sediments. We expected that IP measurements would reduce the ambiguity in interpretation inherent in resistivity and electromagnetic methods. Hydrogeological concerns were the primary incentive of this investigation, as water supply in Denmark relies upon exploitable aquifers within the unconsolidated sediments. Small amounts of clay can greatly reduce hydraulic conductivity. The presence or absence of clayey layers also exerts a fundamental control on the engineering properties of these subsurface sediments.

IP measurements were made at five sites. In this study, results of 1D IP sounding and 2D IP imaging at a site on the Beder aquifer, an important source of water for Aarhus City, are presented. The geophysical data are correlated with logging results obtained using the Ellog system, a resistivity, natural gamma and in-situ pore water sampling system built into the drill auger flights (Christensen and Sorensen, 1998).

Electrical measurements were made using instrumentation as described in Slater and Lesmes (this volume). A Phoenix V5 receiver was used for multi-channel data acquisition. 1D sounding data were inverted for a vertical distribution of resistivity and chargeability using software developed by Sandberg (1996). The 2D dataset was inverted using software developed by LaBrecque (1991). To supplement field IP results, and to further investigate the relationship between IP and lithologic properties, laboratory measurements on samples spanning the broad range of sediments encountered within Aarhus County were made. Grain size distribution and hydraulic conductivity were obtained for each sample. IP response was investigated over the frequency range 0.01-1000 Hz.

Results

The result of the 1D Schlumberger resistivity/IP sounding is shown in Fig. 1 and correlated with resistivity ($|r|$) and natural-gamma counts obtained using the Ellog system. In this environment high gamma counts are known to be associated with clays disseminated in sand, silt and gravel. We expect such clayey (disseminated) sands/silts to have a large IP effect. The 1D inversion result is shown to the right of the lithologic section, with resistivity, chargeability (M) and normalized chargeability (M_n) shown. Normalized chargeability is an absolute measure of the polarization ($M_n = M/|r|$), directly proportional to imaginary conductivity; in contrast, M is a measure of polarization relative to ohmic conduction (see Slater and Lesmes, this volume).

The 1D sounding does not have sufficient resolution to distinguish the numerous clayey layers identified as high counts in the gamma log. However, the layer boundaries modeled by the inversion correlate well with the general shape of the gamma log. Boundaries are modeled at 0.6, 2.2 and 9.4m (the boundary at 66 m is not well constrained).

As previously discussed, lithological characterization from resistivity alone is complicated by the strong dependence of resistivity on fluid chemistry and saturation, in addition to microgeometry and mineralogy. We expect IP to reduce ambiguity in lithological characterization, as microgeometry and clay mineralogy exert strong controls on IP. The clayey sediments from 0.5 – 8 m, identified from the gamma log, are resolved as two layers (Layers 2 and 3) in the inversion. Layer 3, (7.3 m thick) has low $|r|$ and high M_n . However, Layer 2 (1.6 m thick) is modeled as high $|r|$ and high M_n . On the basis of resistivity alone, this layer would not be interpreted as clayey sediment, and the boundary with the upper sand would be incorrectly interpreted as 2.2 m. In contrast, the high M_n in Layer 2 is consistent with the gamma log. Basing our interpretation on M_n , the top of the clayey sediment is correctly predicted at 0.6 m. The higher $|r|$ of Layer 2 may be a result of a change in fluid chemistry or saturation in the near surface. The first layer is modeled with high $|r|$ and low M_n , indicating sediment with low clay content, consistent with the gamma log. Below 9.4 m the model also predicts high $|r|$ and low M_n , again indicating relatively clay free sediments. The clayey layers from 10-11 m and 12-16

m and thinner layers at depth are not resolved in the 1D inversion, due to inadequate resolution using these surface measurements.

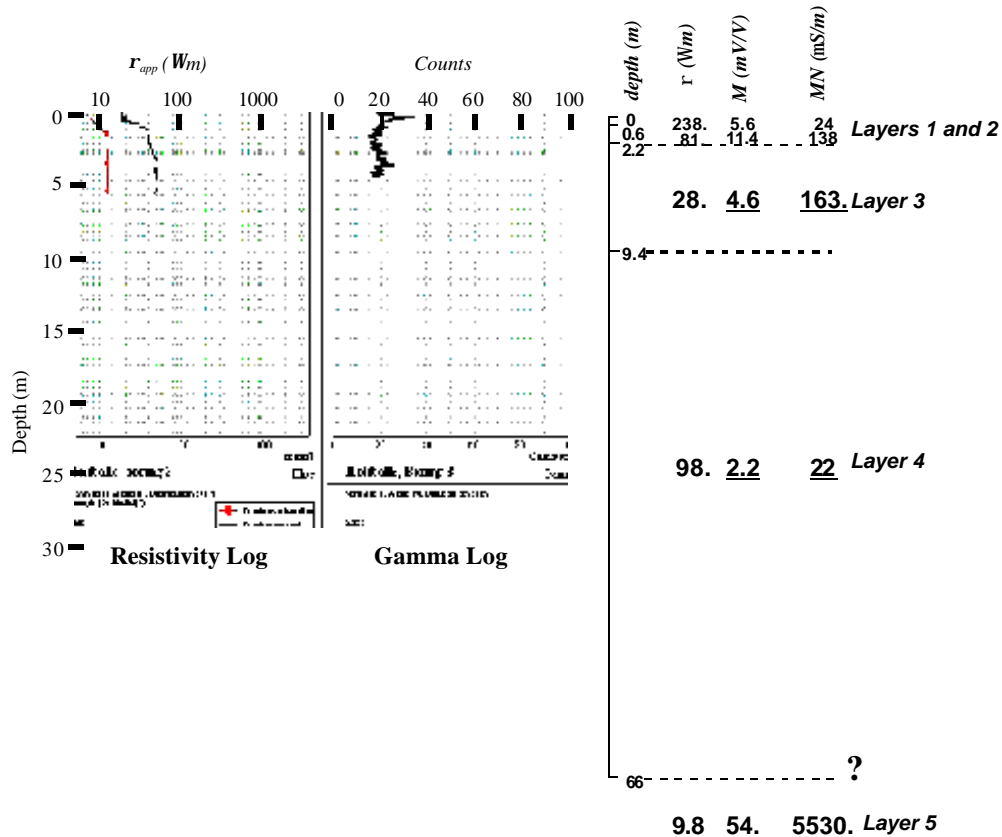


Figure 1: Results of 1D IP sounding on Beder aquifer, Denmark, correlated with Ellog results.

Results of the 2D imaging are presented in Fig. 2. The center of the 1D sounding is at Rb3, 164 m along the line. The resolution of the dipole-dipole array used is not sufficient to resolve Layers 1 and 2 of the 1D sounding. Instead, $|r|$ below Rb3 is imaged as 30-40 Ωm , consistent with Layer 3 of the sounding. Similarly, M_n is 200-250 $\mu\text{S/m}$, again consistent with Layer 3 of the sounding. The imaging just senses the bottom of the clayey sediments identified at 8 m from the gamma log, as indicated by the lower M_n below 7.5 m.

Results of a second Ellog survey at Rb5 indicate that lateral variability in lithology exists at this site. The clayey sediments identified at Rb3 are not evident at Rb5. The M_n image suggests that this layer pinches out between Rb3 and Rb5. Between 25-80 m along the line the clayey layer is only resolved as 2-3 m thick. At Rb5 M_n reaches low values, indicating absence of the clayey layer, as supported by the Ellog results. In contrast, it would be difficult to identify the lithological difference between these sites based on $|r|$ alone. Both sites are imaged with low $|r|$, one possible misinterpretation being that clayey sediments directly underlie both sites. The resistivity structure reflects the dependence on $|r|$ on fluid chemistry and saturation, in addition to lithology. In this case, the M_n image best defines the variation in depth to base of the clayey sediment along the line. The strong M_n resolved at 10 m is the response to a buried metal wire identified by Ellog drillers. It serves as an illustration of the complexities to IP interpretation that may arise in the presence of metal. In the absence of ground truth information, it would be tempting to interpret this IP response as indicative of a local accumulation of clayey material.

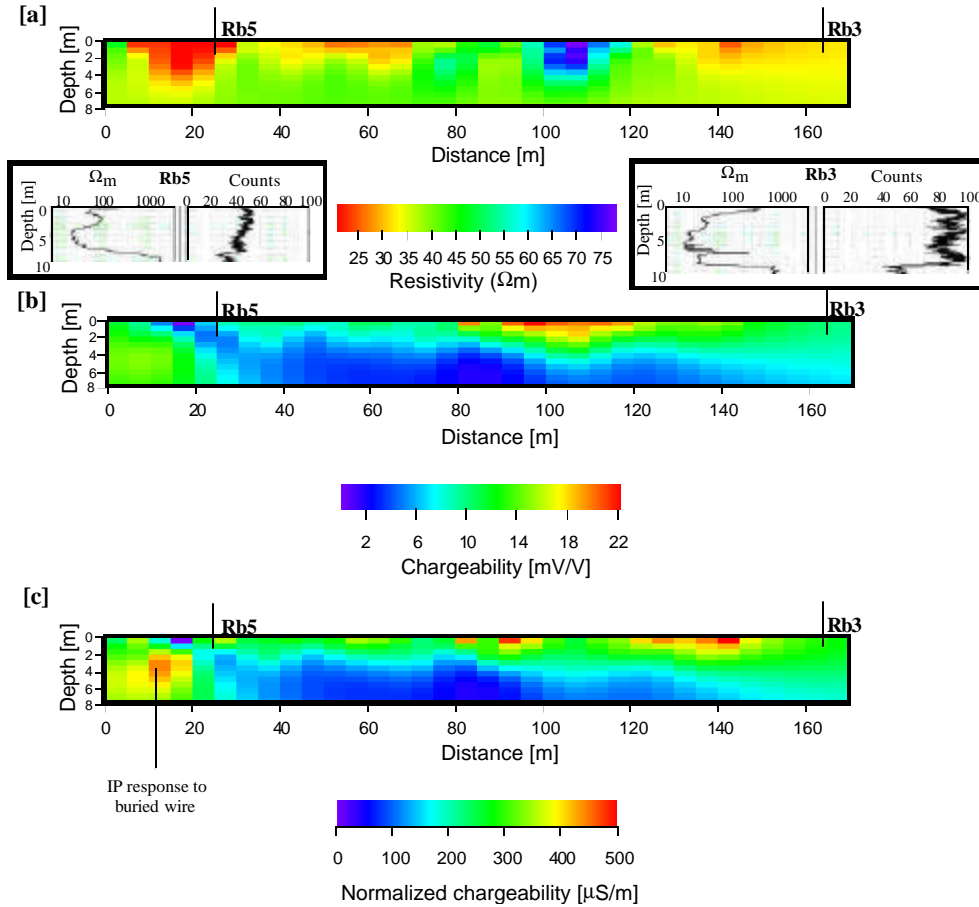


Figure 2: Results of 2D resistivity and IP imaging between Ellog wells Rb3 and Rb5 [a] resistivity [b] chargeability [c] normalized chargeability. Upper 10 m of Ellog wells shown for comparison.

Table 1: Aarhus County lab samples.

Sample	Description	Porosity	Hydraulic Cond. (m/day)
B3-8	Sandy Till – Gravel	0.44	0.0289
B3-14	Clayey Till – Sandy (Hard)	0.65	0.0377
B4-10	Clayey Till – Sandy - few smaller stones	0.54	0.31
B4-14	Coarse Sand and Gravel - few small stones	0.37	179.65
B4-21	Gravel Mixed with fine Materials	0.34	3.33
B4-30	Tertiary Clay with Mica	0.65	0.0226

Given the strong dependence of IP on structure, the possible determination of hydraulic conductivity (k) from electrical measurements has been identified (Weller and Börner, 1996; Börner et al., 1996). Laboratory measurements of IP and k were made on unconsolidated samples collected at sites in Denmark. These samples ranged from gravel to clay (Table 1). The correlation between imaginary conductivity (s'') (polarization) and k is plotted in Fig. 3. The data reveal a strong linear relationship between logarithm of s'' and logarithm of k . Electrical-hydraulic relationships in unconsolidated sediments are currently being investigated in detail. The applicability of IP for determination of k is further considered in the third case study presented here.

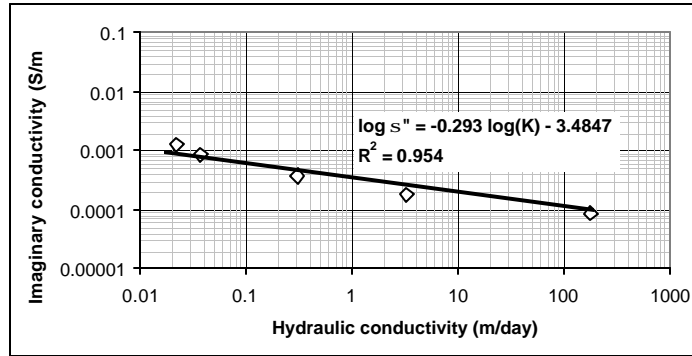


Figure 3: Correlation of imaginary conductivity with hydraulic conductivity obtained for Denmark samples.

3. LITHOLOGICAL CHARACTERIZATION AT THE DRIGG WASTE DISPOSAL FACILITY (UK) USING CROSS-BOREHOLE IP IMAGING

Background

Cross-borehole IP surveys have been performed at the Drigg Low Level Radioactive Waste Disposal Site, Cumbria, UK which is operated by British Nuclear Fuels plc (BNFL). The site is underlain by a complex, heterogeneous sequence of Quaternary sediments, up to 60 m thick in places, which, due to their variability, are difficult to characterize. This complexity is not only attributed to the various glacial and post glacial depositional environments particular to this region of the UK, but also to isostatic loading and unloading associated with ice sheet advance and retreat. BNFL need to characterize these Quaternary deposits in both a geological and hydrogeological sense for a number of reasons. An important engineering requirement is that both buildings and disposal vaults are appropriately constructed. However, BNFL also need to understand the hydrological processes of the sites to assist in location of long-term monitoring boreholes. Furthermore, a radiological risk assessment for the Drigg site requires formulation of a lithological framework to identify potential flow paths.

Trial pits/trenches and borehole investigations have identified vertical and lateral geological variability at the site, making lithological characterization complicated. It is important therefore to supplement borehole and trial pit data with a geophysical program to facilitate correlation between boreholes and trial pits. Frequently, a combination of the lithological types is represented within each stratigraphical unit, complicating correlation between data points. Since many of the main units are expected to have significant contrasts in geoelectrical properties, resistivity and IP imaging may define the degree of continuity between boreholes. The objective of the field trials reported here was to ascertain if IP imaging could successfully characterize Quaternary deposits, especially at an operating waste disposal site.

Results

For the purpose of the investigation two boreholes (labeled BH6124 and BH6125), 15 m apart, were drilled to a depth of 41 m using shell and auger technique. Geological logging revealed a series of sediments which have been classified according to the unit descriptions outlined in BNFL(2000). Table 2 shows the log of each unit for boreholes BH6124 and BH6125 following this classification. Forty-five electrodes were installed in each borehole at 0.8 m intervals over the depth range 5.3 m to

40.5 m. A cross-borehole IP survey was performed using the DMT Resecs instrument, with measurements of resistance (DC resistivity) and phase angle (IP) made using a variety of four electrode configurations. In total, 90 electrodes were used and a total of 5,968 measurements made (50 % used for error checking purposes). Of the 2,984 measurements 1,365 were used for image reconstruction, the others being considered unreliable due to low observed voltages. Image reconstruction was performed using an inversion algorithm outlined by Kemna and Binley (1996) and discussed in more detail in Kemna (2000).

Fig. 4a shows the resistivity image, with natural gamma logs and lithological logs shown for comparison. Note that gamma logs were not available along the entire borehole and in borehole BH6124 natural gamma was only recorded to approximately 12 m depth. The image of resistivity magnitude is consistent with the geological logs, in terms of expected resistivities and lateral connectivity of identified units of similar geoelectrical properties. A number of resistivity contrasts are seen, which correlate with major identified lithological boundaries shown in Table 2. Most noticeable is a marked contrast in near surface clayey units and the underlying unsaturated sands. In addition, the saturated fluvial outwash sands between 16 and 24 m show lower resistivity than the overlying unsaturated sediments. The image also shows two distinct, continuous and relatively resistive units between 25 to 30 m and 32 to 36 m, which form part of the lower glacial till sequence. The sandstone is characterized by a reduction in resistivity when compared with the values determined for the overlying glacial sediments. Correlation with the gamma logs throughout the entire profile is clearly seen.

Fig. 4b shows the IP image (in this case phase angle) between boreholes BH6124 and BH6125. This image correlates with the image of resistivity and indicates that subtle changes in IP distinguish the main units (characterized in Table 2) with a marked contrast at the upper boundary of the sandstone. The near surface clayey sediments exhibit a low polarizability, as expected for highly compacted clays (Vanhala, 1997). A slight reduction in phase angle with increasing saturation is seen in the Fluvial Outwash Formation sand units. Contrasts in polarization magnitude are better shown in terms of imaginary conductivity (which is directly proportional to normalized chargeability used in the previous study). Increased polarization is seen at the base of the sands between 20 to 23 m, correlating with increased natural gamma response (Fig. 4c). Although the glacial tills in the Main Diamict Formation between 24 to 36 m have a similar phase angle to that of the sands above, a marked contrast in imaginary conductivity is apparent. Note that the natural gamma logs in the near surface clayey sediments and the glacial tills show similar counts. The different IP responses reflect the physical (pore size distribution, for example), and likely mineralogical, variations between these units, due to differences in origin and nature of deposition.

The sequence of unconsolidated units at the site shows marked variability in geoelectrical response. IP measurements, when combined with resistivity, can help distinguish different lithological units. IP will not remove all ambiguities in DC resistivity surveys since IP parameters are a function of particle size and mineralogy as well as, to a lesser degree, saturation and pore water chemistry.

Table 2: Summarized geological log of borehole BH6125 and BH6124.

Unit classification following BNFL(2000)	Approximate depth interval (meters below ground level)	
	BH6125	BH6124
Holocene/Recent Formation	0 - 2.0	0 - 2.0
Lacustrine/Fluvial Formation	2.0 - 5.9	2.0 - 5.8
Pebbly Clay Formation	5.9 - 10.7	5.8 - 10.4
Fluvial Outwash Formation	10.7 - 24.5	10.4 - 24.2
Main Diamict Formation	24.5 - 35.9	24.2 - 35.7
Weathered Sandstone	35.9 - 36.2	35.7 - 36.0
Ormskirk Sandstone Formation	36.2 - 41.2	36.0 - 40.7

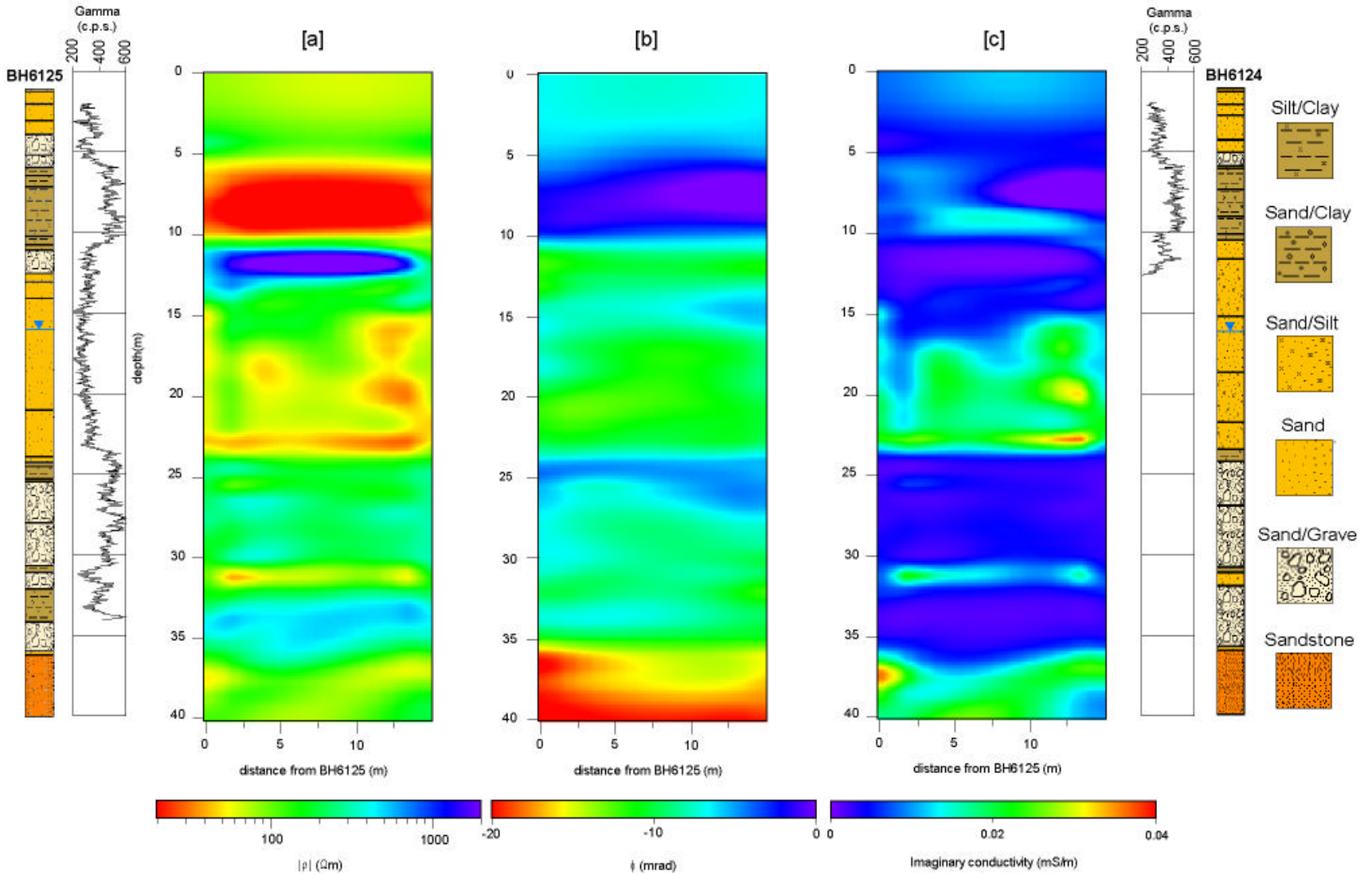


Figure 4: Cross borehole imaging results from Drigg site showing [a] resistivity magnitude, [b] phase and [c] imaginary conductivity. Geological logs and natural gamma logs shown for comparison. All depths below ground level.

4. LITHOLOGIC, ENVIRONMENTAL, AND HYDRAULIC CHARACTERIZATION OF A SEDIMENTARY ENVIRONMENT AT A FORMER JET FUEL DEPOT

Background

In this study, we illustrate the potential of IP for hydrocarbon detection and hydraulic permeability estimation, in addition to lithologic characterization as discussed in the previous examples. This site is a kerosene-contaminated military site near to the Strasbourg-Entzheim airport in France. Principal contamination of the site occurred during operation as a jet fuel (kerosene) depot in the years from its installation in 1957 until the early seventies. Geologically, the area is characterized by a sequence of alluvial sediments associated with the nearby rivers Rhine and Bruche. The stratigraphic situation at the site, inferred from recent drillings, is shown in Fig. 5.

The jet fuel contamination was assumed to have followed the typical migration pattern of a light non-aqueous phase liquid (LNAPL). Generally, LNAPL moves downward under gravity through the unsaturated zone until it encounters either a low permeability formation or the groundwater table. Lateral spreading may occur in the direction of dip of the lithologic barrier (gravity driven) or in the direction of ground-water flow (hydraulically driven). An extensive investigation program conducted in the years 1972 to 1977, which included the installation of multiple monitoring wells, confirmed such LNAPL movement at this site. This study found 400,000 m² of contamination, with accumulations occurring on top of a low-permeability clayey silt layer, located just above the water table (see Fig. 5). Mean hydrocarbon concentrations in this region were determined as about 1 g/kg.

In 1997, resistivity and IP imaging was conducted at the site by DMT, Germany, in order to investigate the practical value of the method for lithologic characterization, hydrocarbon detection, and hydraulic permeability estimation in a sedimentary environment. For this purpose, several, about 13 m deep, boreholes were drilled, with each pair of adjacent boreholes, separated by about 8m, defining a 2D image plane. Sixteen equally spaced copper electrodes were installed in each borehole, with an electrode separation of 0.75 m. Additional electrodes were placed at the surface between boreholes (see Fig. 5). Resistivity and IP (phase angle) data were collected using a Zonge PC-controlled acquisition system (for system details see Daily et al., 1996). For each image plane, all possible dipole-dipole combinations, with a fixed dipole length of two electrode separations, were measured. Data errors were determined from reciprocal measurements, whereby current and potential dipoles are switched. Resistivity and IP images were calculated using an inversion scheme originally proposed by Kemna and Binley (1996) and further described in Kemna (2000). We present selected results that illustrate the value of IP imaging for understanding lithology, hydrogeology and contamination at this site. A detailed description of the study site, field survey results and inverse modeling applied here is given in Kemna (2000).

Results

Lithology and hydrocarbon detection

Fig. 5 shows the inversion result for a selected image plane. The resistivity image basically reflects the lithologic stratification at the site as known from the drillings. The conductive (15-35 Ω m), about 1 m thick clayey silt layer at a depth of approximately 9m is clearly delineated. Underneath, the saturated, clayey sand/gravel formation is characterized by medium resistivities (35-80 Ω m). As expected, the unsaturated sand/gravel region above the silt layer exhibits distinctly higher resistivities (100-1400 Ω m). Due to the high content of clay minerals, the top loessic layer again produces a relatively conductive signature (20-70 Ω m).

Typically, a hydrocarbon contamination is likely to show resistive characteristics. Therefore, the nearly 1 m thick, weakly resistive (250-450 Ω m) anomaly directly above the silt layer may be

associated with the occurrence of kerosene in this region. However, there is no ultimate evidence for this interpretation from the resistivity image alone.

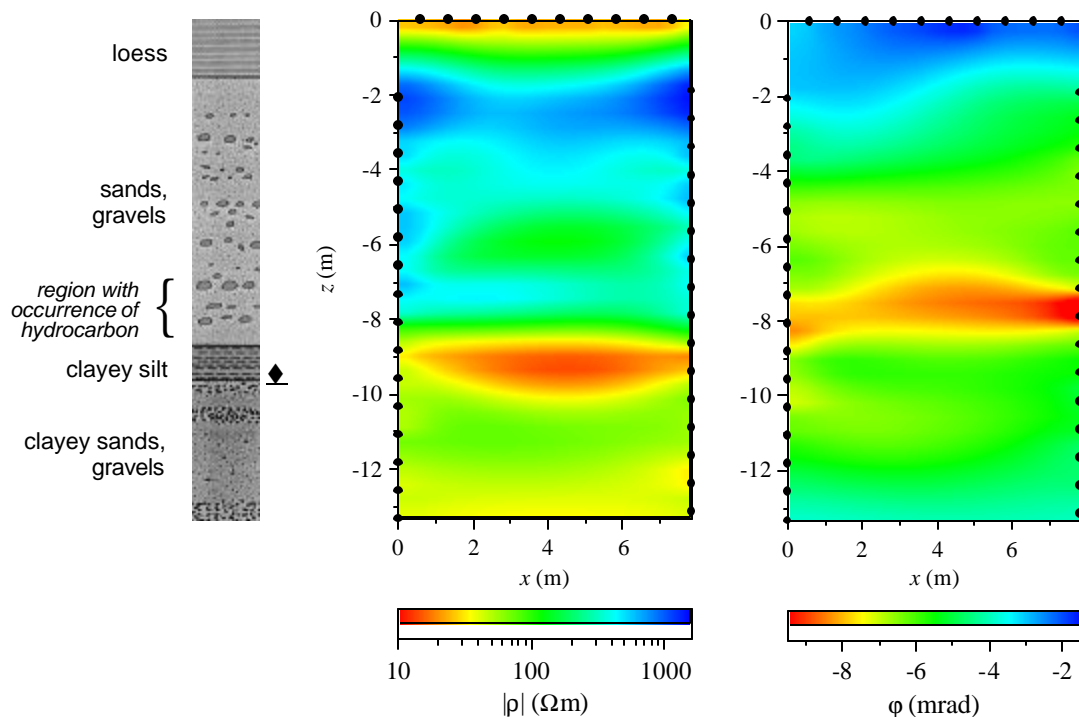


Figure 5: Results of resistivity and IP imaging at the kerosene-contaminated site. In addition to the inverted images of resistivity (middle) and phase (right), the lithologic stratification as determined from cored drillings as well as the occurrence of contamination as proved by chemical sample analyses is shown (left). The solid circles indicate the position of electrodes.

The reconstructed phase image (IP effect) provides additional information on the subsurface. The lowest phase occurs within the top loessic layer (1.5-3.5 mrad). The (clayey) sand/gravel regions are characterized by higher phase shifts (typically 4-7 mrad), whereas the clayey silt layer constitutes a local, weak anomaly of low polarizability. These findings are consistent with results presented by Vanhala (1997) who shows that, in the presence of clay minerals, polarization effects are initially enhanced by increasing dominant grain size. Importantly, the phase image clearly reveals a continuous, roughly 1 m thick layer of increased polarizability (7.5-10 mrad) just on top of the silt layer (coinciding with the weak resistive anomaly in the magnitude image). The results of chemical core sample analyses indicate that this distinct anomaly is caused by hydrocarbon accumulation at this depth.

To support this interpretation, a resistivity/IP survey was conducted in an unpolluted area up-gradient of the military site, with similar geology. The corresponding magnitude and phase results thus serve as control images from a hydrocarbon-free region. This reference survey proved the absence of an increased IP effect directly above the silt layer away from the military site (see Fig. 6), supporting our theory that the hydrocarbon is responsible for the high phase. Note, however, that a different phase behavior is observed within the silt layer itself (see Fig. 6). It therefore appears that the silt horizon is affected by the contamination as well, albeit to a minor degree.

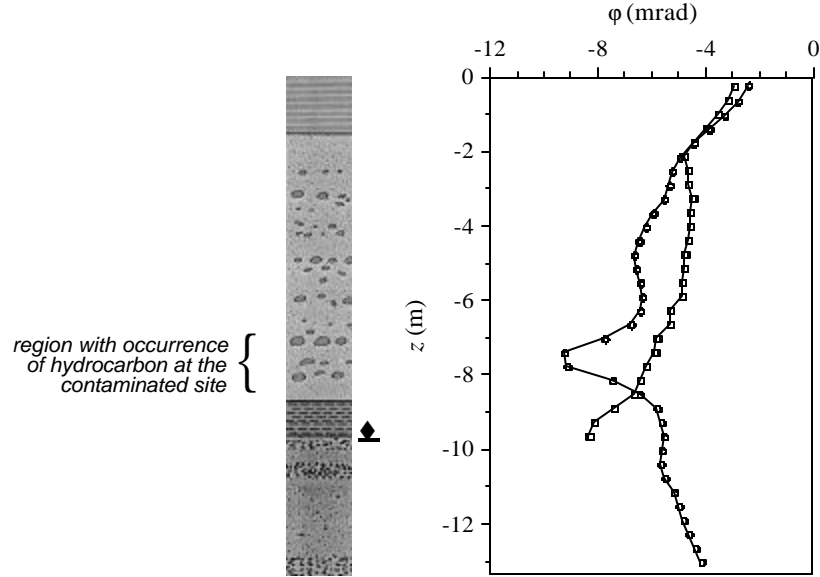


Figure 6: Vertical distribution of phase at the contaminated site (circles) and an uncontaminated reference site (squares) as determined by IP imaging (cf. Fig. 5). Note that, at the reference site, exploration depth is less due to a different electrode setup. The lithologic log, however, reflects the geology at both sites.

A possible explanation of the increased IP effect in the sand/gravel layer might be that the contaminant, as a non-aqueous phase liquid, to some extent obstructs the pore passages. Due to this, the influence of any existing double layers on ion mobility may be increased, ultimately resulting in stronger polarization effects. Note, however, that the numerous laboratory studies on soil and rock samples to date have revealed a range of different possible effects of hydrocarbons on the conduction and polarization properties. These depend on aspects such as contaminant type, water content, clay content, and pore space characteristics. Presently, it is therefore difficult to reliably predict the electrical signature of such contaminants in a given geological environment.

Hydraulic conductivity estimation

Recently, Börner et al. (1996) proposed a promising method for the estimation of one of the key parameters in hydrogeology, the hydraulic permeability (K), from IP measurements. To date, the approach has been restricted to laboratory studies on soil and rock samples, or simple field surveys such as electrical soundings. With the availability of imaging techniques, however, it is now possible to apply the scheme in a tomographic way at the field scale. By this, a continuous image of in-situ K is obtainable, as demonstrated in the following for the present field case.

The estimation procedure is based on the modified Kozeny-Carman equation by Pape et al. (1987), which relates K with the electrical formation factor F and the surface area to pore volume ratio S_{por} . Accordingly, assuming a fractal dimension of the pore surface of 2.36, it is

$$K = \frac{475}{F S_{por}^{3.1}}, \quad (1)$$

where K is in darcies and S_{por} in μm^{-1} . As stated by Börner et al. (1996), S_{por} may be directly calculated from the imaginary component of complex conductivity s'' according to

$$S_{por} = 86 s'', \quad (2)$$

with again S_{por} in μm^{-1} and s'' in mS/m. Provided that pore water conductivity s_w and saturation S_w are known, F is readily obtained from

$$F = \frac{\sigma_w S_w^n}{\sigma \zeta - \sigma \zeta / l}, \quad (3)$$

where n is the saturation exponent and l is the ratio of the imaginary part to real part of pure interfacial conductivity (note that ζ denotes real part).

Although s_w may vary considerably, for the present study it was assumed to be constant. A mean value of $s_w = 108$ mS/m was determined from measurements in three boreholes. As parameters n and l are not directly measurable, typical values for loose sediments were adopted. The values chosen here were $n = 2$ and $l = 0.1$ (see Börner et al., 1996). Uncertainty in the formation factor also exists due to the varying water saturation in the different stratigraphic units. Hence, a simple but plausible saturation model $S_w(z)$ was used to describe the expected situation with depth z (see Fig. 7).

On the basis of the equations and parameters above, a hydraulic permeability image was determined from the IP inversion result of Fig. 5, as shown in Fig. 7. It is evident that the recovered image reflects the given sedimentary sequence. Both the clayey silt layer and top loessic layer, for instance, are clearly delineated in terms of lower K values. The estimated K values suggest that the clayey silt layer does not represent a long-term hydraulic barrier to water or hydrocarbon transport. This is in accordance with the actual situation at the site, since dissolved contaminant components have been detected in the ground water below.

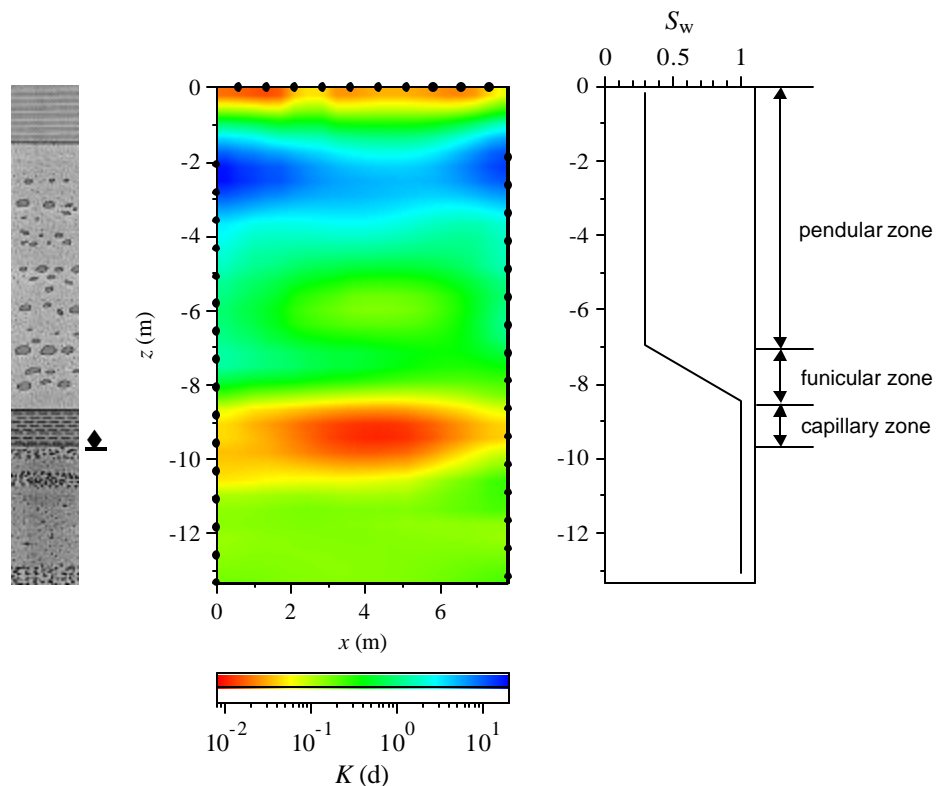


Figure 7: Distribution of hydraulic permeability (middle) as estimated from the IP inversion result (see Fig. 5). The corresponding lithologic log (left), and assumed variation of water saturation with depth (right) are shown. The solid circles indicate the position of electrodes.

The present example proves the general feasibility of K estimation from combined resistivity and IP imaging under realistic field conditions. With appropriate tomographic inversion schemes, such as those employed herein, theoretical relations between intrinsic hydraulic and electrical characteristics can be effectively extended to the field scale. This emphasizes the potential of IP imaging in engineering and environmental studies.

5. DISCUSSION

Our studies encompass the broad range of identified engineering applications of IP imaging. We feel that further fundamental investigations of the dependence of the IP effect on key lithological parameters are required. In particular, the relationship between IP effect and clay content and mineralogy merits further investigation. Previous laboratory studies suggest that it is difficult to resolve clean gravel and coarse sand from compacted clay using IP, as both are characterized by a small IP response (Vanhala, 1997). Such ambiguity could easily lead to misinterpretation of the engineering properties of the subsurface. Resistivity measurements may help to resolve such ambiguity. IP imaging is effective when the range of lithological variation is limited. It is well suited to resolving varying clay content in gravel/sand/silt sequences. In such environments the clay is often disseminated through the sediment and the IP effect increases with increasing clay content. In addition, studies show that the IP effect is closely related to mean grain size of such sediments (Vanhala, 1997). However, at some point the clay content will presumably increase to such a level that, in terms of electrical response, it will behave as a compacted clay. At this point, the IP effect will decrease with further increase in clay content. Our review of the literature indicates that this transition is poorly defined and varies with mineralogy (Telford et al., 1990). It is probably also dependent on microgeometry of the non-clay fraction. Ogilvy and Kuzmina (1972) reported maximum IP effects for disseminated clay contents between 3-8 %. However, Slater et al. (2000) reported polarization to increase with clay content in sand-bentonite mixtures up to 15 % clay content (the highest percentage measured).

These difficulties are reflected in our case studies. In the first study, high polarization correlates with increased clay content as inferred from gamma logs. In these gravel to silt sediments, we assume that the clay is disseminated throughout the sediment. In this case then, IP interpretation is relatively simple. The lithology at the second site is more complex, containing fluvial and glacial sediment types, as well as bedrock. Although changes in IP correlate with major lithologic boundaries, lithologic interpretation on the basis of the IP images is difficult, as no simple relationship between IP response and clay content exists. Instead the IP response is probably a complex function of changes in microgeometry and mineralogy, with secondary fluid chemistry and saturation effects superimposed. We anticipate that such complications will be resolved as the IP method continues to be utilized in engineering studies.

Our third study highlights the potential value of IP imaging for detection of hydrocarbon contaminants and estimating hydraulic conductivity. Both applications are relevant to engineering studies, the design of transportation structures and storage facilities in particular. Hydraulic conductivity is a fundamental parameter that controls how fluid is transported within the subsurface. Images of hydraulic conductivity variability are significant when considering the effects of consolidation and compression of sediments following emplacement of surface structures. Contaminant detection and monitoring technologies are essential at any facilities where hydrocarbons are stored and transported. Despite the need for further work to better understand the physical significance of the IP response, our studies demonstrate the potential value of IP imaging to engineering studies. Given the increasing availability of new data acquisition technology, as well as imaging algorithms, we encourage further engineering related field tests of the method.

6. ACKNOWLEDGEMENTS

Part funding was provided by the Department of Energy and The Maine Science and Technology Foundation via Cooperative Agreements 97-01 DOE, and 98-01. Stewart Sandberg (University of Southern Maine) supervised fieldwork in Denmark, provided the model interpretation of the sounding data and generally encouraged this project. Lee Slater also thanks Kurt Sorensen (Geophysical Laboratory, Earth Sciences, Aarhus University, Denmark) for providing the borehole log for the Beder field site. University of Southern Maine intern students Dan Glaser and Tony Robinson assisted with field data collection. The work at Drigg was carried out under contract A813613 between Lancaster University and BNFL. Rob Gordon and Matthew Randall (BNFL, Risley) are acknowledged for their support with this work. Peter Winship (Lancaster University) helped with data collection at Drigg. The application of IP at the Strasbourg-Entzheim site, France was part of a research project sponsored by the European Environment and Climate Programme (contract ENV4-CT95-0079). We are grateful to the Deutsche Montan Technologie GmbH, Essen, Germany (DMT, GeoTec Division) for approval to present the results in this paper.

7. REFERENCES

- BNFL, 2000, Status Report on the Development of the 2002 Drigg Post-Closure Safety Case, British Nuclear Fuels plc Report, March 2000.
- Börner, F. D. and Schön, J. H., 1991, A relation between the quadrature component of electrical conductivity and the specific surface area of sedimentary rocks: *The Log Analyst*, **32**, 612-613.
- Börner, F. D., Schopper, J. R., and Weller, A., 1996, Evaluation of transport and storage properties in the soil and groundwater zone from induced polarization measurements: *Geophysical Prospecting*, **44**, 583-601.
- Christensen, N. B. and Sorensen, K. I., 1998, Surface and borehole electric and electromagnetic methods for hydrogeological investigations: *European Journal of Environmental and Engineering Geophysics*, **3**, 75-90.
- Daily, W. D., Ramirez, A. L., and Zonge, K., 1996, A unique data acquisition system for electrical resistance tomography: *Proc. Symp. Application of Geophysics to Engineering and Environmental Problems, Environ. Eng. Geophys. Soc.*, 743-751.
- Kemna, A., 2000, Tomographic inversion of complex resistivity - theory and application, PhD Thesis, Ruhr University Bochum, Germany, 176pp.
- Kemna, A. and Binley, A., 1996, Complex electrical resistivity tomography for contaminant plume delineation: *Proc. 2nd Meeting of the Environmental and Engineering Geophysics Society – European Section*, 196-199.
- Klein, J. D., and Sill, W. R., 1982, Electrical properties of artificial clay-bearing sandstone: *Geophysics*, **47**, 1593-1605.
- LaBrecque, D. J., 1991, IP tomography: 61st Ann. Internat. Mtg., Soc. Expl. Geophys., Expanded Abstracts, 413-416.
- Ogilvy, A. A. and Kuzmina, E. N., 1972, Hydrogeologic and engineering-geologic possibilities for employing the method of induced potentials: *Geophysics*, **37**, 839-861.
- Olhoeft, G. R., 1985, Low-frequency electrical properties: *Geophysics*, **50**, 2492-2503.
- Pape, H., Riepe, L., and Schopper, J. R., 1987, Theory of self-similar network structures in sedimentary and igneous rocks and their investigation with microscopical and physical methods: *J. Microscopy*, **148**, 121-147.
- Poulsen, L. H. and Christensen, N. B., 1999, Hydrogeophysical mapping with the transient electromagnetic sounding method: *European Journal of Environmental and Engineering Geophysics*, **3**, 201-220.
- Sandberg, S. K., 1996, Microcomputer software for individual or simultaneous inverse modeling of transient electromagnetic, resistivity, and induced polarization soundings: New Jersey Geological Survey Open-File Report OFR 90-1, 160pp.
- Slater, L. and Lesmes, D., The induced polarization method, this volume.

- Slater, L., Lesmes, D. and Sandberg, S. K., 2000, IP interpretation in environmental investigations: Proceedings of the Symposium on the Application of Geophysics to Engineering and Environmental Problems, 935-944.
- Sturrock, J. T., Lesmes, D. and Morgan, F. D., 1998, The influence of micro-geometry on the hydraulic permeability and the induced polarization response of sandstones: Proceedings of the Symposium on the Application of Geophysics to Engineering and Environmental Problems, 859-867.
- Telford, W. M., Geldart, L. P. and Sheriff, R. E., 1990, Applied Geophysics, Second Edition, Cambridge University Press, Cambridge, 770pp.
- Vanhala, H., 1997, Mapping oil-contaminated sand and till with the spectral induced polarization (SIP) method, Geophysical Prospecting, **45**, 303-326.
- Vanhala, H., Soininen, H. and Kukkonen, I., 1992, Detecting organic chemical contaminants by spectral-induced polarization method in glacial till environment: Geophysics, **57**, 1014-1017.
- Vanhala, H. and Soininen, H., 1995, Laboratory technique for measurement of spectral induced polarization response of soil samples: Geophysical Prospecting, **43**, 655-676.
- Vinegar, H. J. and Waxman, M. H., 1984, Induced polarization of shaly sands: Geophysics, **49**, 1267-1287.
- Weller, A. and Börner, F. D., 1996, Measurements of spectral induced polarization for environmental purposes: Environmental Geology, **27**, 329-334.